ELSEVIER

Available online at www.sciencedirect.com
SCIENCE DIRECT®

Journal of Crystal Growth 273 (2005) 458–463

JOURNAL OF CRYSTAL GROWTH

www.elsevier.com/locate/jcrysgro

Investigation of Mn-implanted n-Si by low-energy ion beam deposition

Lifeng Liu[a,*], Nuofu Chen[a,b], Shulin Song[a], Zhigang Yin[a], Fei Yang[a], Chunlin Chai[a], Shaoyan Yang[a], Zhikai Liu[a]

[a]*Key Laboratory of Semiconductor Materials Science, Institute of Semiconductors, The Chinese Academy of Sciences, Beijing 100083, China*

[b]*National Laboratory of Micro-Gravity, Institute of Mechanics, The Chinese Academy of Sciences, Beijing 100083, China*

Received 1 April 2004; accepted 8 September 2004
Communicated by M. Schieber
Available online 19 October 2004

Abstract

Mn ions were implanted to n-type Si(0 0 1) single crystal by low-energy ion beam deposition technique with an energy of 1000 eV and a dose of $7.5 \times 10^{17}\,cm^{-2}$. The samples were held at room temperature and at 300 °C during implantation. Auger electron spectroscopy depth profiles of samples indicate that the Mn ions reach deeper in the sample implanted at 300 °C than in the sample implanted at room temperature. X-ray diffraction measurements show that the structure of the sample implanted at room temperature is amorphous while that of the sample implanted at 300 °C is crystallized. There are no new phases found except silicon both in the two samples. Atomic force microscopy images of samples indicate that the sample implanted at 300 °C has island-like humps that cover the sample surface while there is no such kind of characteristic in the sample implanted at room temperature. The magnetic properties of samples were investigated by alternating gradient magnetometer (AGM). The sample implanted at 300 °C shows ferromagnetic behavior at room temperature.
© 2004 Elsevier B.V. All rights reserved.

PACS: 81.05.Ea; 81.05.Zx; 81.15.Hi; 82.80.Pv

Keywords: A1. Auger electron spectroscopy; A1. X-ray diffraction; A3. Low-energy ion beam deposition; B2. Semiconducting silicon

1. Introduction

Diluted magnetic semiconductors (DMSs) combine the electronic transport properties of semiconductors and the memory characters of

*Corresponding author. Tel.: +86 10 82304569; fax: +86 10 82304588.
E-mail address: lfliu@red.semi.ac.cn (L. Liu).

0022-0248/$ - see front matter © 2004 Elsevier B.V. All rights reserved.
doi:10.1016/j.jcrysgro.2004.09.039

magnetic materials and are important to develop spin-controlled electronic devices and integrated magnetic device applications. Nowadays, the investigation of diluted magnetic semiconductors has received a great deal of attention. The most extensively studied and most thoroughly understood materials of diluted magnetic semiconductors are $A_{1-x}{}^{II}$ Mn_xB^{VI} and $A_{1-x}{}^{III}$ Mn_xB^{V}, in which Mn replaces a fraction of group II or III sublattices randomly [1–4]. But, group IV (such as Si and Ge)-based diluted magnetic semiconductors may result more practical for applications since present semiconductor technology may be used [5–7].

It is well known that the maximum solid solubility of transition metal ions in silicon at thermal equilibrium is very low. Therefore, the non-equilibrium doping process is necessary to realize the high doping concentration. Silicons heavily doped with transition metal manganese at the doping levels more than 5% have been successful grown by using gas–source molecular beam epitaxy (GSMBE) [8,9] and laser-ablation molecular beam epitaxy (LAMBE) [10]. Hwa-Mok Kim et al. reported on the growth of ferromagnetic Mn_xSi_{1-x} films by vacuum evaporation method, in which the Curie temperature of $Mn_{0.07}Si_{0.93}$ is 210 ± 5 K [11]. Yokota et al. reported the fabrication of single-phase Ce_xSi_{1-x} films and their magnetic and electrical transport properties, and also examine the annealing effects, which vary the crystallographic state of the host Si and the coordination of Ce [12]. However, Si-based DMSs have not been fully investigated.

In this paper, the characteristics of Mn-implanted n-type Si by low-energy ion beam deposition were investigated. The structure and surface morphologies of samples were analyzed by X-ray diffraction (XRD) and atomic force microscopy (AFM) while the atomic concentrations of samples dependence on the depth were studied by Auger electron spectroscopy (AES). The magnetic properties of samples were investigated by alternating gradient magnetometer (AGM) at room temperature.

2. Material preparation

The samples were prepared by low-energy dual ion beam deposit system with the mass selection function, which can purify the ions and even select isotopes to implant into the substrate. Mn ion beams were produced by Bernas-type ion source. More detailed information was elaborated about this apparatus in Ref. [13]. Only one ion beam system was employed to implant Mn ions into the substrate in this experiment. N-type Si (0 0 1) were used as substrate, which were cleaned in ethanol, acetone, and deionized water for 5 min each with ultrasonic vibration, then they were etched in FH/H_2O solvent. Finally, they were rinsed in deionized water and loaded into the growth chamber. The vacuum was $<10^{-6}$ Pa in the chamber. The substrate was annealed at 800 °C for 30 min before growth in order to further eliminate the oxidation layer. Through mass-selection in magnetic field and acceleration in electric field, Mn ions were uniformly implanted into silicon substrate at high dose of $7.5 \times 10^{17}\,cm^{-2}$ with low-energy of 1000 eV. The samples were held at room temperature (sample A) and at 300 °C (sample B) during the implantation.

3. Measurements and analyses

3.1. Compositional analyses

AES was employed for analyzing the surface composition of samples and their compositional variation along the cross section. The AES system used in this experiment is SAM PHI-610.

Fig. 1 is the AES spectra of the samples surfaces, which show that there are manganese, silicon, carbon and oxygen at the samples surfaces. The samples depth profiles are shown in Fig. 2. It can be seen from Fig. 2 that the concentrations of the oxygen and carbon are very high at the samples surfaces and decrease rapidly along the depth. The reason for the existence of carbon is that the samples surfaces were contaminated after the samples were taken out from the growth chamber. The element oxygen is introduced by oxidation of manganese after the samples were removed from the growth chamber. The manganese atomic concentration of sample A reaches the maximum of 18% at the depth of 6 nm, and quickly drops down from the maximum point, whereas that of

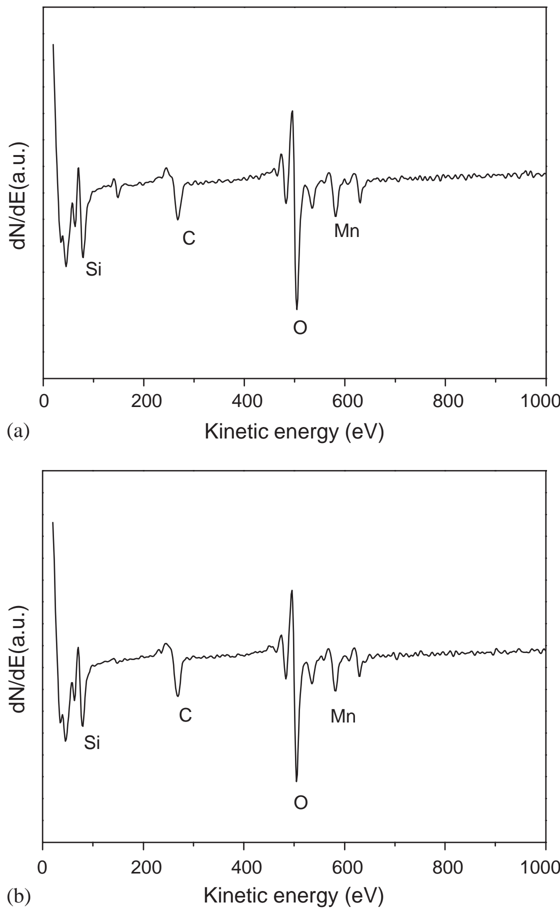

Fig. 1. AES spectra at the samples surfaces: (a) sample A and (b) sample B.

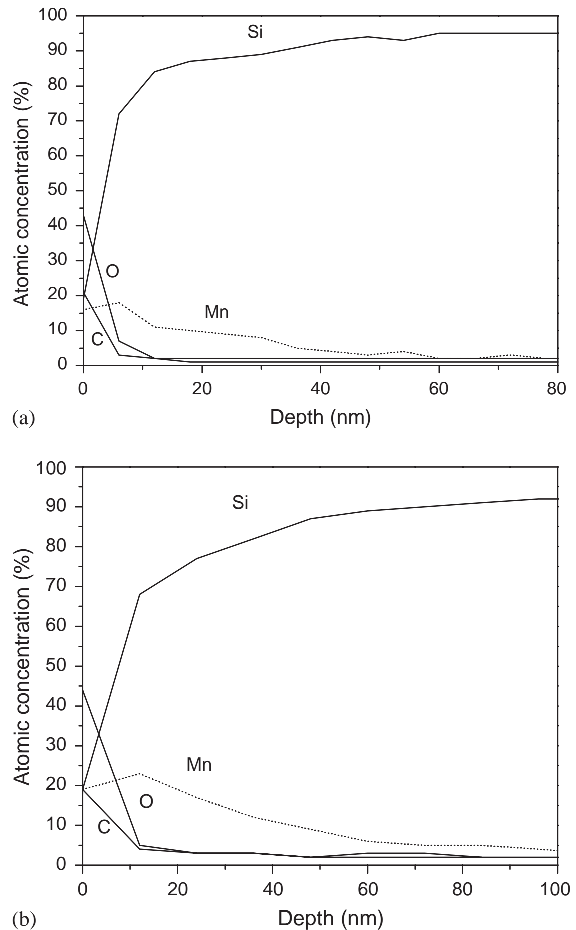

Fig. 2. AES depth profiles for samples: (a) sample A and (b) sample B.

sample B reaches the maximum of 23% at the depth of 12 nm, and slowly drops down. It indicates that the Mn ions reach deeper in sample B than in samples A. The dose of manganese ions in samples A and B is identical. They were held at different temperature during implantation. So, the substrate temperature affects the implantation depth of manganese ions. During the analyzed depth area, the manganese atomic concentration of sample A is fluctuant after the maximum while that of sample B monotonically decreases. It shows that there is a segregation of manganese atoms in sample A. The segregation of manganese atoms is suppressed in sample B.

3.2. Structural analyses

The structural properties of samples were studied by X-ray diffraction measurements. The XRD patterns of samples were measured with a Rigaku diffractometer using Cu Kα radiation for structural analyses. The wide range of the XRD (20–80°) patterns are shown in Fig. 3. The XRD spectra of samples A and B are shown in Figs. 3(a) and (b), respectively. In sample A, only Si(0 0 1) substrate peak is observed. The forbidden peak of Si(0 0 2) appears in sample B. The structure of sample A is amorphous due to the heavily Mn ions implantation at room temperature. As the substrate temperature is elevated to 300 °C in sample

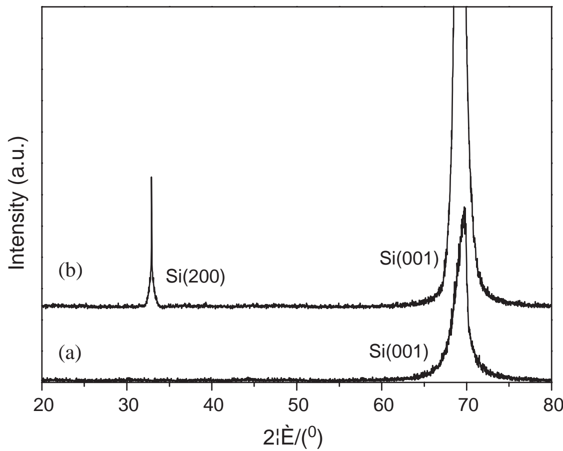

Fig. 3. XRD spectra of samples: (a) sample A and (b) sample B.

B, the crystal structure of sample is restored. Stacking faults are introduced by the recrystallization process and result in the appearance of Si(0 0 2) forbidden peak [14]. There are no additional diffraction peaks except for Si in both samples A and B. We have carefully searched for secondary phases such as Mn or Mn silicides. However, no such phases are observable.

3.3. Morphological analyses

AFM is a noninvasive technique to deliver three-dimensional realistic impressions of the measured sample surface. It is an easy and fast method to show the change in the amplitude of the surface roughness. The surface morphologies of samples were observed by AFM. Figs. 4(a) and (b) show the surface morphology of samples A and B, respectively. It can be seen that the surface morphology of samples A and B is quite different. There are many island-like humps on the sample B surface with a RMS of 12.231 nm on a $5 \times 5\,\mu m$ surface scanning area. There is no such kind of characteristic on sample A surface. The surface of sample A is much smooth with a RMS of 0.635 nm. The surface roughness is in close relationship with the sample structure. The AFM results indicate that the crystal structure of sample A is amorphous while that of sample B is crystallized. The AFM results are consistent with the XRD profiles.

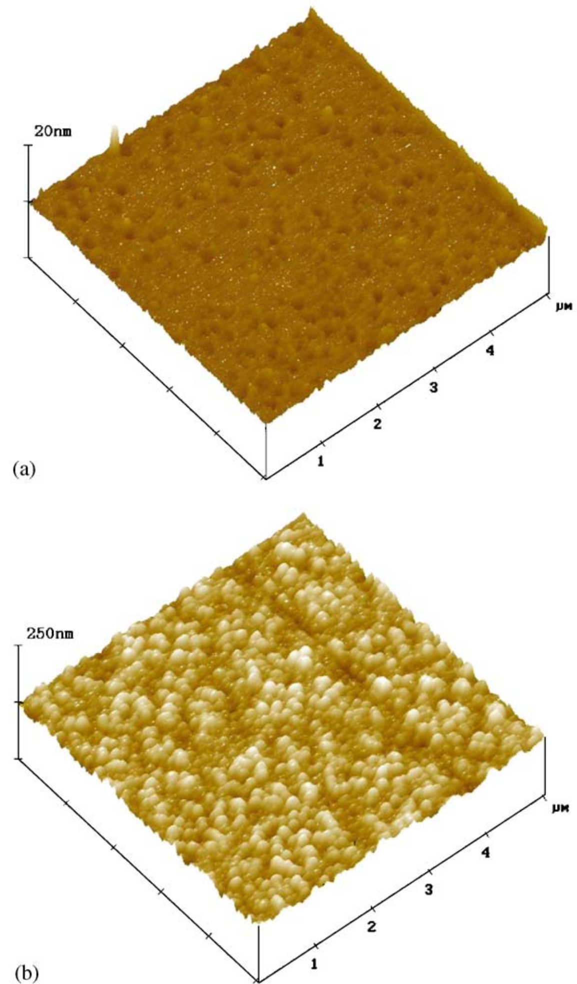

Fig. 4. AFM morphologies of samples: (a) sample A and (b) sample B.

3.4. Magnetic analyses

The magnetic properties of samples were measured on a Model 2900 MicroMag^{TM} AGM at room temperature. The results of the magnetization measurements by AGM reveal room-temperature ferromagnetism for sample B while no ferromagnetism can be observed for sample A. Fig. 5 shows the ferromagnetic hysteresis loop of

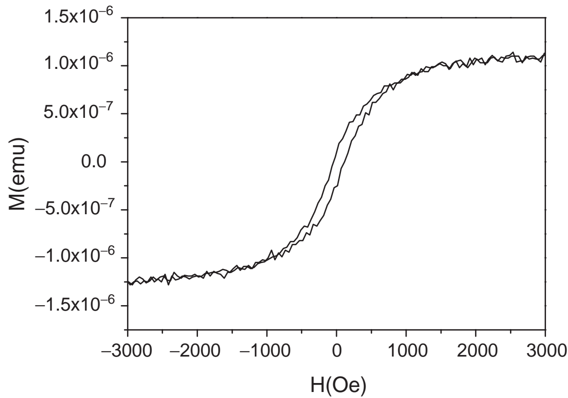

Fig. 5. Ferromagnetic hysteresis loop of sample B measured by Alternating gradient magnetometer at room temperature.

sample B. The magnetization curve is obtained with the applied field parallel to the sample plane. The diamagnetic background contribution due to Si is subtracted from the data. The coercivity H_C and saturation magnetization M_S of sample B are about 75.68 Oe, and 1.298×10^{-6} emu, respectively.

Pure Si does not have a net magnetic moment, resulting in diamagnetism. Metallic Mn is antiferromagnetic, with a Néel temperature of 100 K [15]. In addition, nearly all of the possible Mn-based binary and ternary oxide candidates are antiferromagnetic. Only the Mn_3O_4 is ferromagnetic with a Curie temperature of 42 K [15]. Furthermore, only one of all the Mn–Si compounds is ferromagnetic with a Curie temperature of 38 K [16]. However, they could not account for the room-temperature ferromagnetic behavior of sample B due to low Curie temperature. Diluted magnetic semiconductor Mn_xSi_{1-x} is ferromagnetic. The Curie temperature of ferromagnetic Mn_xSi_{1-x} film by vacuum evaporation method has reached 210 ± 5 K [11]. The magnetic properties of Mn_xSi_{1-x} have not been fully investigated until now. From the XRD result of sample B no new phases are found. It is possible that Mn_xSi_{1-x} structure is formed in sample B. But, we cannot make sure if the room-temperature ferromagnetism of sample B is related to Mn_xSi_{1-x} structure before making further investigation on it.

4. Summary

The characteristics of Mn-implanted n-type silicon were investigated. The structure of sample A is amorphous while that of sample B is crystallized. There are no new phases found except silicon in all the samples. Sample B has island-like humps that cover the sample surface while sample A has a much smoother surface. Samples AES depth profiles show that the Mn ions reach deeper in sample B. Room-temperature ferromagnetic behavior shows in sample B though further investigation is still needed.

Acknowledgements

This work was partially supported by the National Natural Science Foundation of China (Grant no. 60176001, 60390072) and Special Funds for Major State Basic Research Projects of China (Grant no. 20000365, 2002CB311905).

References

[1] H. Ohno, A. Shen, F. Matsukura, A. Oiwa, A. Endo, S. Katsumoto, Y. Iye, Appl.Phys.Lett. 69 (1996) 363.
[2] M.L. Reed, N.A. El-Masry, H.H. Stadelmaier, M.K. Ritums, M.J. Reed, C.A. Parker, J.C. Roberts, S.M. Bedair, Appl. Phys. Lett. 79 (2001) 3473.
[3] A. Haury, A. Wasiela, A. Arnoult, J. Cibert, S. Tatarenko, T. Dietl, Y. Merle dAubigné, Phys. Rev. Lett. 79 (1997) 511.
[4] X. Liu, U. Bindley, Y. Sasaki, J.K. Furdyna, J. Appl. Phys. 91 (2002) 2859.
[5] Hiroshi Nakayamaa, Hitoshi Ohtab, Erkin Kulatovc, Physica B 302–303 (2001) 419.
[6] A. Stroppa, S. Picozzi, A. Continenza, A.J. Freeman, Phys.Rev. B. 68 (2003) 155203.
[7] Y.D. Park, A.T. Hanbicki, S.C. Erwin, C.S. Hellberg, J.M. Sullivan, J.E. Mattson, T.F. Ambrose, A. Wilson, G. Spanos, B.T. Jonker, Science 295 (2002) 651.
[8] Hiroshi Nakayamaa, Hitoshi Ohtab, Erkin Kulatov, Physica B 302–303 (2001) 419.
[9] H. Nakayama, H. Ohta, E. Kulatov, Thin Solid films 395 (2001) 230.
[10] S. Abe, Y. Nakasima, S. Okubo, H. Nakayama, T. Nishino, H. Yanagi, H. Ohta, S. Appl. Sur. Sci. 142 (1999) 537.
[11] Hwa-Mok Kim, Nam Mee Kim, Chang Soo Park, Shavkat U. Yuldashev, Tae Won Kang, Kwan Soo Chung, Chem. Mater. 15 (2003) 3964.

[12] T. Yokota, N. Fujimura, T. Ito, Appl. Phys. Lett. 81 (2002) 4023.
[13] F.-G. Qin, X.-M. Wang, Z.-K. Liu, et al., Rev. Sci. Instrum. 62 (1991) 2322.
[14] T. Yokota, N. Fujimura, Y. Morinaga, T. Ito, Physica E 10 (2001) 237.
[15] D.P. Norton, S.J. Pearton, A.F. Hebard, N. Theodoropoulou, L.A. Boatner, R.G. Wilson, Appl.Phys.Lett. 82 (2003) 239.
[16] T. Takeuchi, M. Igarashi, Y. Hirayama, M. Futamoto, J. Appl. Phys. 78 (1995) 2132.